PERGAMON

Chemical Engineering Science 57 (2002) 497–506

Chemical Engineering Science

www.elsevier.com/locate/ces

Visualization and numerical simulation of fine particle transport in a low-pressure parallel plate chemical vapor deposition reactor

Heru Setyawan, Manabu Shimada, Kenji Ohtsuka, Kikuo Okuyama *

Department of Chemical Engineering, Graduate School of Engineering, Hiroshima University, 1-4-1 Kagamiyama, Higashi-Hiroshima 739-8527, Japan

Received 9 May 2001; received in revised form 23 August 2001; accepted 18 September 2001

Abstract

The behavior of fine particles in a low-pressure parallel plate chemical vapor deposition reactor was investigated by constructing a system that permits particle motion in the reactor to be visualized. The test spherical silica aerosol particles, which were 1.0 μm in diameter and dispersed in argon gas, were fed into the reactor from the outside and particle motion was detected by a laser light scattering method. The effect of operating conditions, such as pressure and temperature, on particle transport in the reactor was investigated. The pressure was varied from 2.0 to 4.0 Torr and the wafer-substrate plate temperature was varied over the range of 25 °C to 300 °C. A three-dimensional numerical simulation was performed using the commercially available computational fluid dynamics code Fluent. A detailed configuration of the reactor, including the showerhead structure was considered when investigating this mechanism. It is found, both experimentally and by numerical simulation that, when the wafer-substrate plate is not heated, the effect of pressure on particle trajectory in the space between plates cannot be observed. However, at elevated temperature, i.e. when the wafer-substrate plate is heated, the particle trajectory is apparently influenced by pressure. In addition, the effect of thermophoresis, as the result of a temperature gradient by heating of the wafer-substrate plate is very pronounced for gas pressures of both 2.0 and 4.0 Torr. The experimentally observed phenomena were satisfactorily reproduced by simulation.

Keywords: CVD reactor; Particle contamination; Reduced pressure; Light scattering; Numerical simulation; Dynamic behavior

1. Introduction

Chemical vapor deposition (CVD) processes are commonly used to produce thin films in the microelectronics industry. Particle contamination becomes a major factor in these types of processes, since it causes severe problems during the production of the thin films. A major problem is pattern defects, which represent the main cause of yield reduction. Possible contamination sources include dirty gas lines, poor loading procedures, homogeneous gas phase nucleation, and flaking of the chamber surface material. Fine particles, which are generated during the deposition processes, represent one of the leading causes of defects and reduced yields, and because of this, the focus of particle contamination control in the microelectronics industry is increasingly shifting from the clean room environment to the process tools themselves (Okuyama, Huang, Seinfield, Tani, & Kousaka, 1991; Okuyama, Huang, Seinfield, Tani, & Matsui, 1992; Rao et al., 1998). Thus, preventing particle generation during the deposition process is an issue of major importance. However, it is very difficult or even impossible to completely eliminate particle generation in such a process. Hence, controlling particle transport in the reactor in such a way so that the particles are deposited on surfaces other than the substrate is important. This is possible if we have a better understanding of the dynamics of particles in a fluid. Therefore, it is indispensable to develop a better physical understanding of the nature of fine particle transport in CVD reactors in order to eliminate contamination in the process equipment. In addition, product requirements are pushing the semiconductor industry in the direction of low-pressure processes (Choi, Rader, & Geller, 1996). Consequently, it is also important to understand particle transport under low-pressure operating conditions, since particle behavior under these conditions can be significantly different from higher-pressure processes.

* Corresponding author. Tel.: +81-824-24-7716; fax: +81-824-24-7850.

E-mail address: okuyama@hiroshima-u.ac.jp (K. Okuyama).

0009-2509/02/$ - see front matter
PII: S0009-2509(01)00373-6

A parallel-plate type reactor is one of the widely used reactors in CVD processes. Particle transport in the reactor may be governed by a variety of mechanisms, including convection, diffusion, external forces and inertia (Adachi & Okuyama, 1998). Particle diffusion is important for small particles and/or at low pressure. Particle inertia is responsible for the deviation of the particle trajectories from the gas streamlines in the space between the plates. Schmidt, Fissan, and Schmidt (1996) showed that inertia has a strong effect on particle deposition in cases where small distances exist between the particle point injection and a surface. External forces can include gravity, electrical and thermophoresis. Gravity is an important force for the case of larger particles. In the large-particle limit, gravity becomes the dominating deposition mechanism (Choi et al., 1996; Garrity, Peterson, Garret, & O'Hanlon, 1995). Electric forces play an important role in dictating the transport of charged particles in the presence of electric field, such as in plasma processing tools. Thermophoresis may be significant in the presence of temperature gradients and plays an important role in particle deposition on semiconductor wafers (MacGibbon, Busnaina, & Fardi, 1999; Oh, Yoo, & Myong, 1996; Ye et al., 1991). The above workers showed that particle deposition could be reduced by increasing the temperature gradient between the wafer and walls including the showerhead. In addition, thermophoretic force also plays an important role in particle transport during the postplasma regime and keeps the particles moving away from the wafer (Collins, Brown, O'Hanlon, & Charlie, 1995).

There are two fundamentally different approaches for calculating particle transport dispersed in a gas flow in a parallel-plate reactor, and are referred to as the Lagrangian (Garrity et al., 1995; Choi et al., 1996) and Eulerian (Nijhawan, McMurry, & Campbell, 2000; Oh et al., 1996) methods. In the Lagrangian method, the particle force balance is integrated numerically along particle trajectories to give a particle velocity field. In the Eulerian method, the particle equations are solved in Eulerian form. This method allows similar techniques to be used both for a gas flow field and for particle trajectories. However, as pointed out by Slater and Young (2001), this method has difficulties relative to the implementation of particle boundary conditions at solid surfaces because the Eulerian equations cannot simultaneously convey information in two or more directions. This suggests that such a method cannot represent any degree of particle reflection. In addition, this method will experience ill-posed when individual particle pathlines cross, since in the particle equations, information can only travel through the computational domain in the direction of the particle pathlines.

All reported studies concerned with particle transport in a parallel plate CVD reactor have analyzed the particle transport mechanisms using a simplified reactor geometry. The gas flow in the space between plates was treated as the stagnation point flow. The results were then characterized in terms of collection efficiency. The agreement between the spatial distribution of the number concentration of particles or the particle trajectories does not become an important issue as long as the collection efficiency is in good agreement (Nijhawan et al., 2000). There is no study which has addressed the issue of particle behavior in such a reactor by taking into account details of reactor configuration such as showerhead, baffle, and related items. In order to properly control particle contamination, details of the fluid flow in a given reactor configuration should be considered since the behavior of the particles is strongly dependent on the fluid flow field. In addition, there is no reported study in which the particle trajectories obtained from numerical simulation are compared to those from particle visualization experiments.

In this present work, we wish to report on a study of the behavior of fine particles in a low-pressure parallel plate-type CVD reactor by taking into account the details of reactor configuration, as well as of fluid flow. The role of thermophoretic force was investigated in detail, since it is one of the most important forces that influence fine particle movement in such a reactor. An experimental method to measure particle transport and behavior in the reactor was developed. In this case, inert particles injected from outside into the low-pressure reactor were used so that the particle size could be well defined. A system was developed to deliver particles from a higher-pressure environment to a low-pressure chamber for the purpose of visualization. The particle trajectories in the space between the plates were observed by using a laser light scattering (LLS) technique. A three-dimensional numerical simulation using computational fluid dynamics (CFD) was carried out, in order to elucidate the mechanism of particle transport.

2. Experimental technique and apparatus

Fig. 1 shows a schematic diagram of the experimental apparatus. The main equipment consists of (i) an aerosol generator equipped with pressure reduction system, (ii) a conventional parallel plate-type reactor, and (iii) an LLS system to visualize particle motion. The dimension and configuration of the reactor have been reported elsewhere (Fujimoto et al., 2000). Briefly, the upper plate is a showerhead where gas enters the reactor. It has 145 holes with diameter of 1.0 mm. A baffle that contains 16 holes with diameter of 6.0 mm is installed above the showerhead. The wafer-substrate plate is the position where the substrate being processed is placed, and the temperature is controlled by a controller.

Test spherical silica particles 1.0 μm in diameter were dispersed into argon gas by an aerosol generator (RBG-1000, Tokyo Dylec) prior to feeding into the reactor. The problem encountered in delivering particles from atmospheric pressure into a very low-pressure environment is a tendency of the capillary pressure reducer to be clogged by particles. If this occurs, the continuous supply of particles for the purpose of visualization cannot be guaranteed. In addition, the

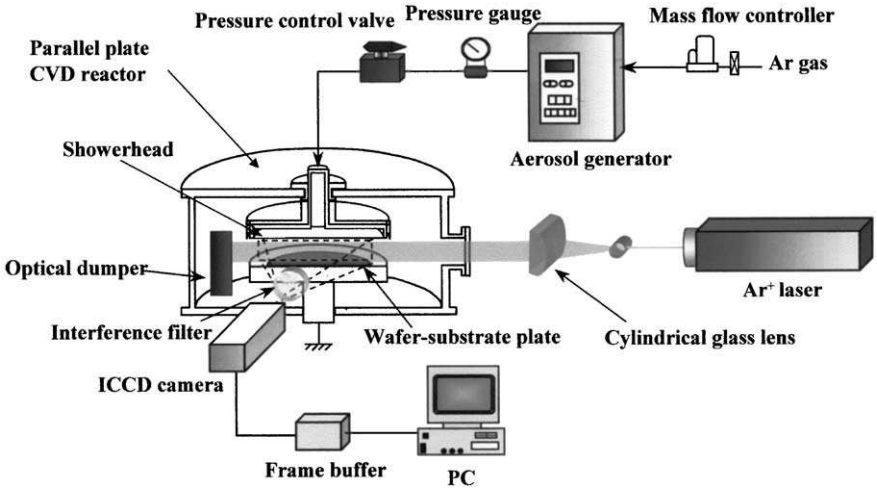

Fig. 1. Schematic diagram of the experimental apparatus and the LLS system used to visualize the particle behavior.

predetermined operating conditions cannot be maintained. Therefore, a pressure reduction system using a pressure control valve was developed to deliver gas–particle mixture from a high-pressure environment to the very low-pressure chamber. This device has been successfully used to study particle behavior in a low-pressure environment.

The volumetric flow rate of the gas in all experiments was set constant at a constant value of 300 sccm by means of a mass flow controller. The operating pressure of the reactor was varied from 2.0 to 4.0 Torr. When thermophoresis effect on the particle transport is not considered, the wafer-substrate plate is not heated. The effect of thermophoresis was investigated by heating the wafer-substrate plate, the temperature of which was set to 300°C. The actual temperature of the plate cannot be represented by a single value since it is difficult to achieve a uniform distribution over the entire surface. Therefore, the temperature distribution was measured using a thermocouple. The temperature distribution of the showerhead and other walls was also measured. The measured and the corresponding fitted lines of the radial profiles of the showerhead and the wafer-substrate plate temperatures are shown in Fig. 2 for a pressure of 2.0 Torr. The same results were obtained for a pressure of 4.0 Torr. The measured wall temperatures were for later use as boundary conditions for numerical simulations.

The spatial distribution of particles was observed by an LLS technique. A laser beam 488 nm in wavelength and approximately 2.0 W in power from an Ar^+ laser (Model-2017, Spectra Physics) was expanded to form a light sheet 33 mm in height and 1 mm in thickness using a rod and a cylindrical lens. The laser sheet was passed through a window of the reactor in order to irradiate the space between the plates, from approximately 1 mm below the showerhead and 1 mm above the wafer-substrate plate. An image intensified charged couple device (ICCD) camera (IMAX 512, Princeton Instruments, Inc.) having an

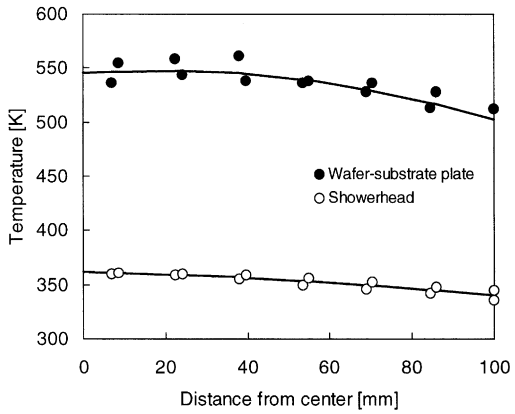

Fig. 2. The measured and the fitted lines for temperature distribution along the radial direction of the showerhead and the wafer-substrate plate. The fitting equations take the form of $T=-1283.0r^2-84.658r+361.79$ for the showerhead and $T=-5678.8r^2+189.06r+547.11$ for the wafer-substrate plate.

interference filter (center wavelength: 488 nm, full-width at half-maximum: 1 nm) was used to detect the light scattered by particles. The signal was passed through a frame buffer and was recorded using a PC.

3. Governing equations and numerical simulation

A numerical simulation was performed using the commercially available CFD code Fluent 5.3 (Fluent, Inc.). The particle trajectories were calculated using a Lagrangian formulation. The individual particle trajectory is tracked by solving the following force balance equations for each particle:

$$\frac{d\mathbf{x}_p}{dt}=\mathbf{u}_p \tag{1}$$

and

$$m_p \frac{\mathrm{d}\mathbf{u}_p}{\mathrm{d}t} = \mathbf{F}_g + \mathbf{F}_D + \mathbf{F}_T, \tag{2}$$

where $\mathbf{x}_p$ and $\mathbf{u}_p$ are the particle position and velocity, respectively. $\mathbf{F}_g$, $\mathbf{F}_D$ and $\mathbf{F}_T$ are the forces acting on the particle due to gravity, fluid drag and thermophoretic forces, respectively. The drag force is calculated according to Stokes–Cunningham law to account for non-continuum effects at low pressures and is written as

$$\mathbf{F}_D = \frac{3\pi\mu d_p}{C_c}(\mathbf{u} - \mathbf{u}_p). \tag{3}$$

The Cunningham slip correction factor C_c is given by

$$C_c = 1 + Kn[1.257 + 0.4\exp(-1.1/Kn)]. \tag{4}$$

Thermophoretic force is calculated based on the equation proposed by Talbot, Cheng, Schefer, and Willis (1980) and is expressed as

$$\mathbf{F}_T = -\frac{6\pi d_p \mu^2 C_s (K + C_t Kn)}{\rho(1 + 3C_m Kn)(1 + 2K + 2C_t Kn)} \frac{1}{T} \nabla T. \tag{5}$$

In the simulation, it is assumed that the particle is sufficiently dilute so that particle–particle interactions and the effects of the particle volume fraction on the gas phase are negligible. Therefore, the particle trajectories can be calculated based on a fixed gas phase flow field obtained prior to the calculation of particle trajectories.

The set of equations that govern for the gas phase flow are described by continuity, momentum and energy equations for a compressible flow. The compressible flow was used because of the large variations in pressure in the reactor, especially in the showerhead structure. Pressure work and kinetic energy are accounted for in the energy equation of compressible flow model. The gas is assumed to obey the ideal gas law. Viscous dissipation is neglected.

The numerical analysis employed to solve the governing equations is based on the finite volume formulation. The simulations were performed in a full three-dimensional mode to take into account the complicated geometry of the showerhead structure. The computational domain was extended from the inlet tube above the showerhead structure to the exhaust line, which is located at the sidewall as shown in Fig. 3(a). Figs. 3(b) and (c) show the enlarged picture and details of the showerhead structure, respectively. The number, diameter and arrangement of holes at the showerhead and baffle are exactly set the same as real ones. In Fig. 3(a), the boundary conditions used in the simulation are also displayed. The no-slip wall condition is applied to the walls. The fluid mass flux at the inlet is specified using a profile for a fully developed flow through a pipe. A pressure outlet boundary condition is used on the exit boundary in which the gauge pressure is set to zero. For heating conditions, in which the energy equation is solved, the measured wall temperatures shown in Fig. 3(a) were used for both pressure of 2.0 and 4.0 Torr.

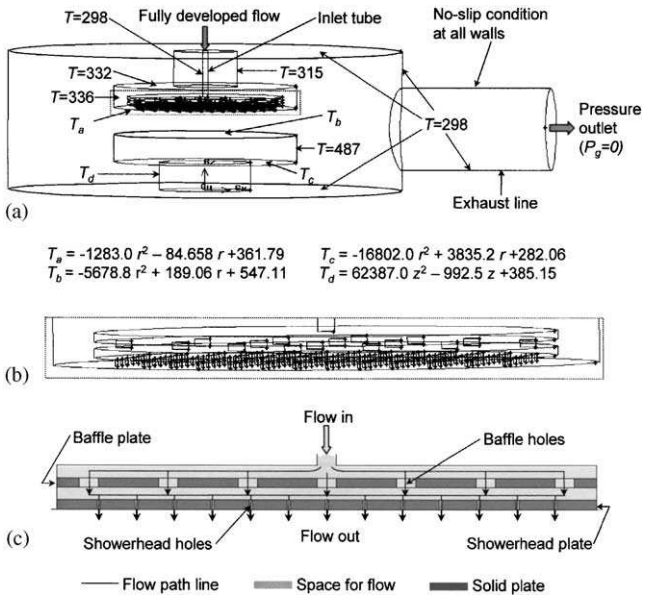

Fig. 3. (a) Computational domain and boundary conditions for the numerical simulation, (b) enlarged picture of the showerhead structure shown in (a), and (c) detail of the showerhead structure. The unit of temperature T shown in this figure is in K. r and z in the fitting equations of temperature profile represent radial and axial positions in m, respectively.

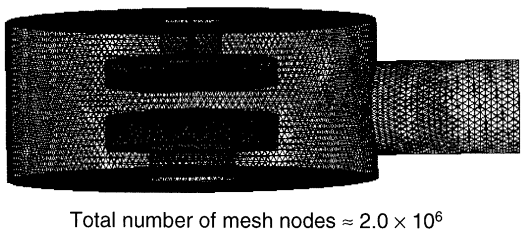

Fig. 4. Unstructured triangular/tetrahedral grid arrangement used in the calculation.

The reactor geometry is represented as unstructured triangular/tetrahedral meshes containing approximately 2.0×10^6 nodes. The grid arrangement is shown in Fig. 4. A mesh size of 2.5×10^{-3} m is applied for the inlet tube, the showerhead structure and the space between the plates, and 5.0×10^{-3} m for the other. The solution of momentum and energy equations is approximated by second order upwind differencing scheme in order to minimize numerical diffusion since, in the triangular/tetrahedral grid arrangement, the grid is not aligned with the flow. The pressure–velocity coupling is treated using the Semi-Implicit Method for Pressure Linked Equations (SIMPLE) algorithm of Patankar (1980).

The particle trajectories are calculated by releasing particles with zero momentum from the inlet surface. This initial condition can be justified since the relaxation time, i.e. the time required for particle to adopt the fluid velocity, of 1.0 μm size particle is approximately 6.196×10^{-8} and 6.123×10^{-8} s for pressures of 2.0 and 4.0 Torr, respectively. Assume that argon gas enters the tube with the

volumetric flow rate of 300 sccm. If the flow is assumed to be fully developed, the maximum gas velocity is approximately 125 m/s at the center axis for pressure 2.0 Torr. Thus, the particle will travel along a distance of about 8.0×10^{-6} m to adopt the gas velocity. This distance is much smaller than the length of the inlet tube. Therefore, it would be expected that the particles have adopted the gas velocity before leaving the tube and entering the showerhead structure so that the calculation of particle trajectory inside the reactor will not be affected by this initial condition. When the particles impinge chamber surfaces, they are assumed to be perfectly absorbed.

4. Results and discussion

4.1. Comparisons of particle visualization and simulation

Fig. 5 shows the particle visualization image in the space between the plates with the corresponding trajectory from simulation for different wafer-substrate plate temperatures and pressures. The slopes of trajectory with an arrow in each image of experiment as well as of simulation are plotted in Fig. 6 to compare the measured and simulated trajectory. The figures were taken at a vertical plane that has an angle of 45° to the axis of the exhaust line. All two-dimensional figures presented hereafter will be given at the same position. For each figure of the visualization image, the upper part corresponds to the showerhead and the lower part to the wafer-substrate plate. The left-hand side is the opposite side of the exhaust port and the right-hand side is the region close to the exhaust port. The brighter image in the irradiating plane represents the existence of particles, while the darker regions denote the absence of particles. Since only a vertical sheet of laser light is used to illuminate the particles, the image is only obtained when the particles pass through the light sheet. No information is available regarding the origin of the particles or their fate. Thus, this illumination technique limits measurements to a single cross section of the particles and it is not possible to obtain a complete three-dimensional structure of the particle trajectories. However, the measurement technique provides useful information regarding particle behavior and dynamics in the space between plates. The effect of operating conditions such as temperature and pressure on particle trajectories can be easily investigated.

To reproduce a two-dimensional image of the experiments from a three-dimensional calculation, the following procedure was carried out. The trajectory of approximately 30,000 particles was calculated in order to obtain a representative pattern. From the total number of particles tracked, about 50% were trapped in the showerhead structure. When a particle being tracked passes through a specified plane, the particle position was recorded. The thickness of the plane is 1 mm, the same as that of the laser sheet, which irradiates the space between the plates. A two-dimensional image of the particles on the plane was then reconstructed. In the simulated particle images, lines that encase an ensemble of particles were added as a visual guide to make the trajectories clearer.

A uniform distribution of particle trajectories can be seen in the simulated images for all operating conditions. This corresponds to the position and the number of the showerhead holes above the top edge of the plane. On the contrary, a uniform distribution cannot be seen in the visualization images. The simulated trajectories were taken in a plane in which the top edge always coincides with a series of showerhead holes that form a line. This differs from the experiments where the top edge of laser sheet does not always coincide with a series of holes that form a line and it may vary from experiment to experiment.

Even though the simulation and the experiment are not precisely the same, however, the same general features can be observed. At ambient temperature, i.e. when the wafer-substrate plate is not heated, the following pattern can be observed both for 2.0 and 4.0 Torr pressure conditions. At the middle part, the particle transport is dominated by the downward direction once the particles enter the reactor through the showerhead holes. At other regions, the particles change their transport direction smoothly. The pattern of the trajectories is similar for 2.0 and 4.0 Torr pressures, suggesting that the particle trajectory is not influenced by the operating pressure for the range of conditions examined herein. This phenomenon was also observed by Nijhawan, McMurry, and Campbell (2000), in that the collection efficiency on the wafer is not influenced by pressure.

When the wafer-substrate plate temperature is set to 300°C, the particle trajectories change significantly from those where no heat was applied, for both 2.0 and 4.0 Torr pressures. A sharp bend can be seen, when the particles approach the wafer-substrate plate. Effect of pressure on particle transport can be observed. The sharper bend is more obvious for a pressure 2.0 Torr as indicated by a more abrupt change in its slope (see Fig. 6). The results show that the experimentally observed phenomena can be satisfactorily reproduced by simulation. The mechanisms of the particle transport will be discussed below.

4.2. Validation of simulations

Before investigating the particle transport mechanisms, it is necessary to verify that the predicted flow field is sufficiently accurate. Since the showerhead structure is the most critical part due to a much smaller length scale compared to the size of the reactor, the pressure drop across the structure was measured in the absence of particles. Fig. 7 shows the measured and the predicted inlet pressure for different chamber pressures ranging from 0.72 to 7.0 Torr. It can be seen that the general trend of the predicted inlet pressure is in good agreement with the measurements.

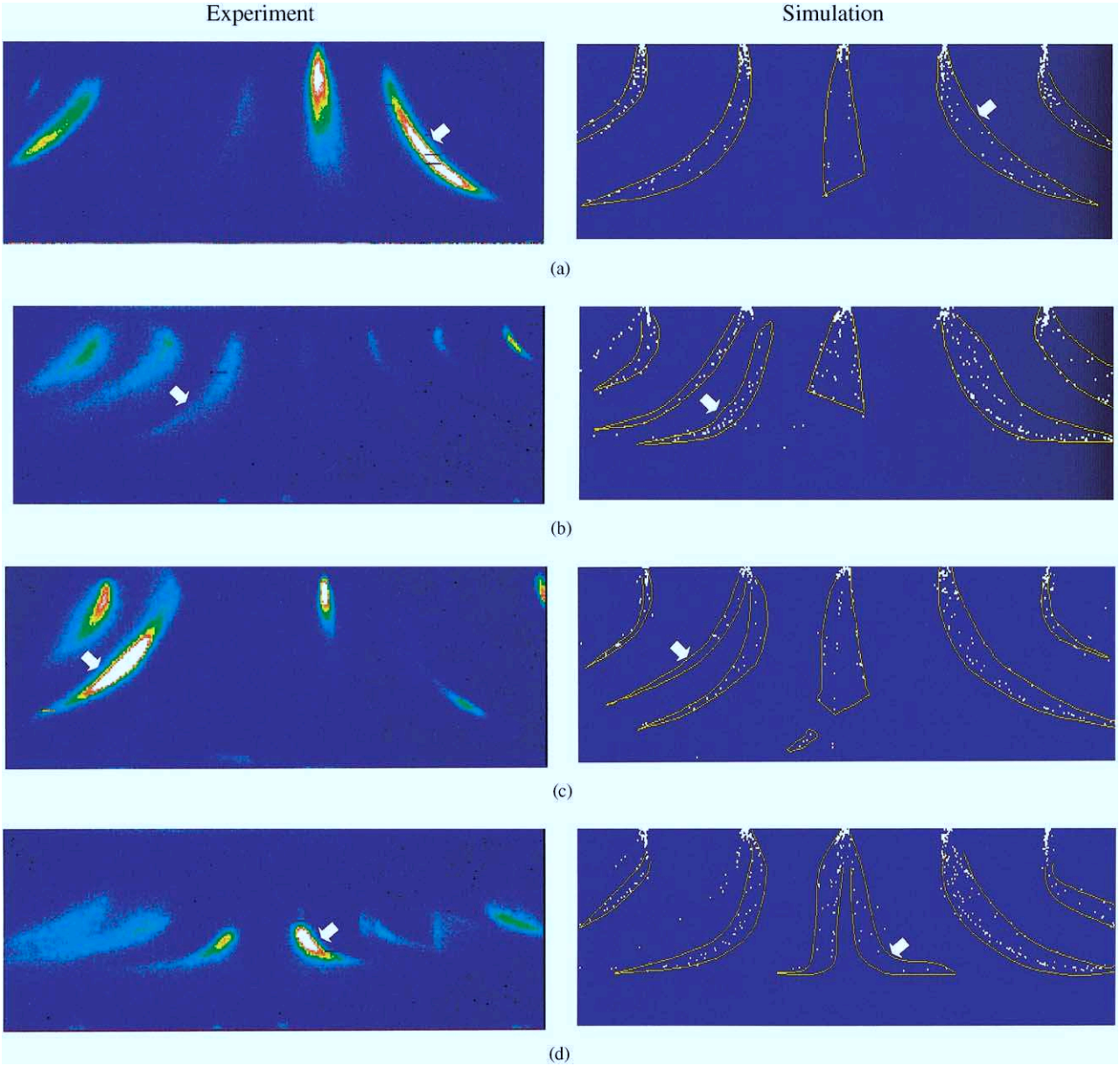

Fig. 5. Comparison of the visualization and the simulated images for particle trajectories in the space between the plates for various operating conditions: (a) reactor pressure 4.0 Torr without heating, (b) reactor pressure 4.0 Torr with heating by setting the wafer-substrate plate temperature to 300°C, (c) reactor pressure 2.0 Torr without heating, and (d) reactor pressure 2.0 Torr with heating by setting the wafer-substrate plate temperature to 300°C. The slopes of trajectory pointed with an arrow are plotted in Fig. 6.

The predicted inlet pressure increases in an almost linear manner with the chamber pressure where there is a sudden change of slope at pressure 2.0 Torr. This trend is consistent with the measurement. The predicted pressure is slightly lower than that of the measured value, which may be caused by the low-pressure conditions. For low-pressure conditions, the continuum fluid approximation becomes less accurate, since the Knudsen number becomes small, i.e. the gas mean free path becomes more comparable to chamber dimensions, especially in the showerhead structure. In addition, since the reactor geometry has features of disparate length scales, the accuracy of the overall calculation may be impeded.

4.3. The simulated flow field

Numerically generated steady state flow field in the space between the plates for a pressure of 4.0 Torr for the case of no heating condition (on the left) and pathlines for the case of no heating and heating conditions (on the right) are displayed in Fig. 8. Even though the overall flow patterns inside the entire reactor are quite different for the case of

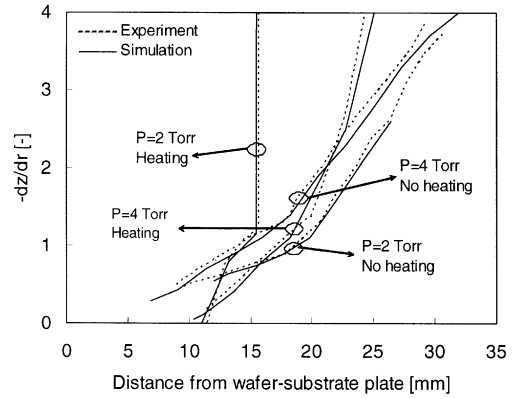

Fig. 6. Change of representative particle trajectory direction in the space between plates as a function of axial distance.

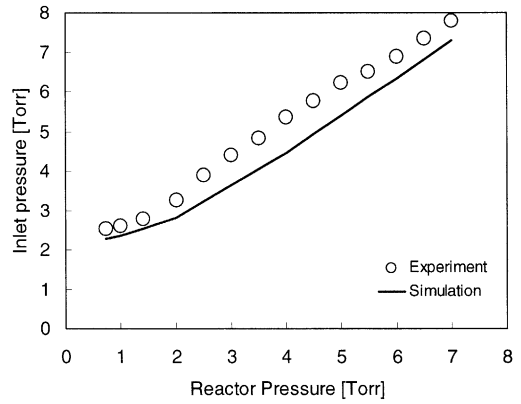

Fig. 7. Comparison of the measured and predicted pressures at the inlet tube for various reactor pressures.

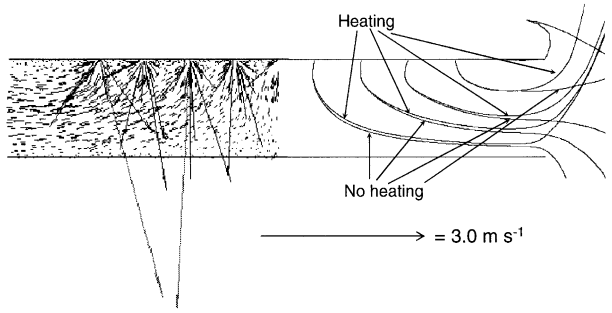

Fig. 8. Simulated gas flow field in the space between the plates for the case of no heating condition (on the left) and pathlines for the case of no heating and heating conditions (on the right). The display of some vectors in the velocity field is omitted to make it clearer. The operating pressure is 4.0 Torr.

no heating and heating conditions, however, the general gas flow patterns in the space between the plates for all conditions examined are similar. It can be seen in Fig. 8 in which the pathlines for no heating condition almost coincide with those of heating conditions. The gas flow enters the space between the plates through the holes of the showerhead, which

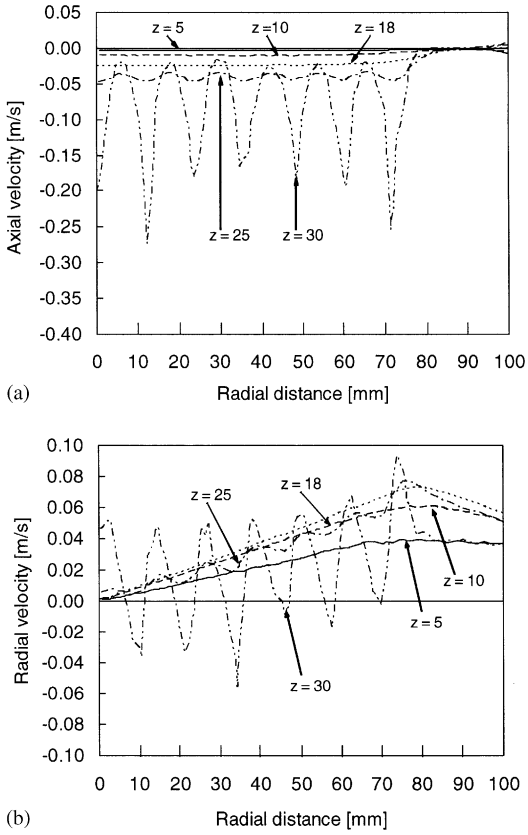

Fig. 9. The velocity profiles along a radial cut at a distance of 5, 10, 18, 25 and 30 mm above the wafer-substrate plate for a pressure of 4.0 Torr and a no heating condition, (a) axial velocity and (b) radial velocity.

accelerates and directs the flow toward the wafer-substrate plate. The velocity decay out so fast once the flow leaves the holes of the showerhead. The flow then bends laterally outward except in the middle region where the dominant velocity direction remains vertically downward. As the flow approaches the wafer-substrate plate, it is deflected at nearly a 90° angle. An area of near stagnation is present in the vicinity of the wafer-substrate plate. For heating conditions, the flow is directed slightly upward when leaving the space between the plates. To clarify this, a radial profile of the axial and radial velocity component at several axial positions in the space between the plates is displayed in Fig. 9 for a pressure 4.0 Torr and no heating condition. At a distance of 30 mm above the wafer-substrate plate (5 mm below the showerhead), the fluctuation in the radial and axial velocities is large. The peak indicates the location of the holes. The radial velocity is nearly zero at the center and then increases along with the radial direction when the effect of the jet diminishes.

4.4. The simulated particle trajectories

A typical illustration of simulated particles trajectories viewed from the bottom is shown in Fig. 10 for a pressure

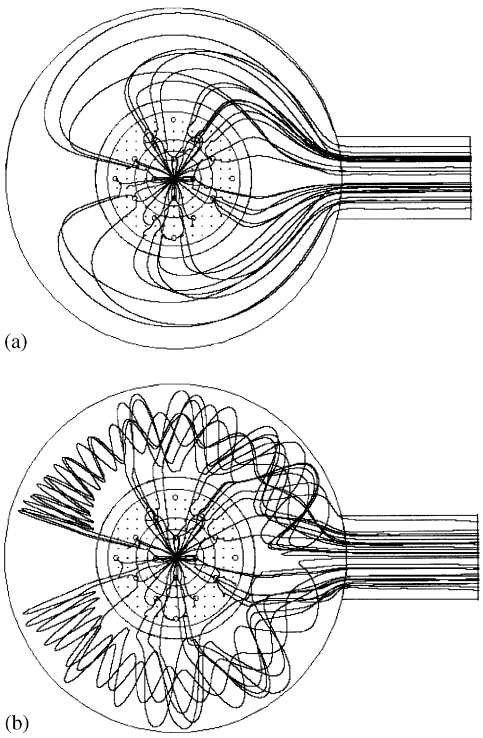

Fig. 10. Bottom view of the simulated particle trajectories for pressure 4.0 Torr: (a) no heating condition, and (b) heating condition by setting the wafer-substrate plate temperature to 300°C.

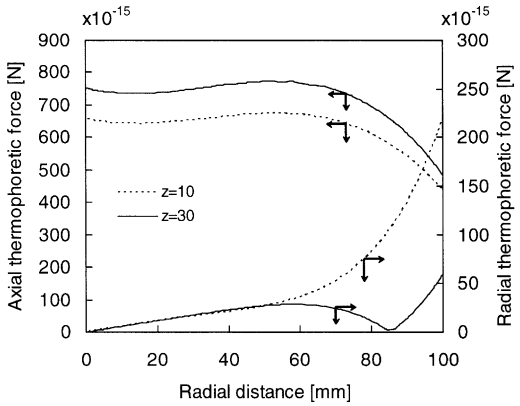

Fig. 11. The axial and radial profiles of the thermophoretic force along a radial cut at a distance of 10 and 30 mm above the wafer-substrate plate for the case of pressure 4.0 Torr and heating conditions by setting the wafer-substrate plate temperature to 300°C.

of 4.0 Torr with the conditions of no heating and heating of the wafer-substrate plate. The particles were initially distributed uniformly on the inlet surface, entering the space between the plates in the reactor through the showerhead and are uniformly distributed in the tangential direction. For no heating conditions, the trajectories are simple. Once the particles exit the space between the plates, they follow the gas flow and proceed directly to the exhaust port. However, when the wafer-substrate plate is heated, the particle trajectories are more complicated. In this case, they travel to the exhaust port in a circulating manner. The flow field for heating conditions outside the space between the plates is quite different from those where no heating is applied. There are extensive circulation flows due to natural convection and the interplay among the forces acting on the particles appears to be complicated.

4.5. The particle transport mechanisms

In this section, the mechanism of particle transport will be examined based on the simulation results. Fig. 11 shows the corresponding axial and radial component of thermophoretic force acting on a particle under the heating conditions at pressure 4.0 Torr. The trend for pressure 2.0 Torr is the same even though the magnitude is higher. The axial thermophoretic force is large at the middle part and then decreases close to the edge of the plates. Compared to gravitational force, the axial component of the thermophoretic force is on the order of approximately 550 higher. The axial drag force is a decreasing function of the distance from the showerhead. Therefore, when a particle approaches the wafer-substrate plate, the influence of the axial drag force becomes smaller and particle transport is dominated by the thermophoretic force. Consequently, a sharp bend is observed in the particle trajectories when the particles approach the wafer-substrate plate. This differs from the no heating condition due to the lack of thermophoresis. In this case, the particles turn smoothly.

The radial component of the thermophoretic force is smaller than that of the axial component, but it is still larger than the gravitational force. At a distance of 10 mm above the wafer-substrate plate, the force is nearly zero at the center and then increases with radial distance. At the center, the temperature gradient is nearly zero. At a distance of 5 mm below the showerhead, the force fluctuates from zero at the center, gradually increasing to a certain level, then decreasing again, and eventually increases almost linearly. The temperature fluctuation is large in the area close to the showerhead. The gas temperature is lower in the area just below the holes since a lower temperature gas enters the reactor with high velocity. Consequently, there is a large fluctuation on the thermophoretic force.

In order to understand more clearly the effect of thermophoresis on particle transport in the reactor, we characterize the particle deposition to a region between radial distance r_i and r_{i+1} $(i=1,N)$ on the wafer as a non-dimensional particle deposition efficiency. It is defined as the fraction of particles entering the reactor that end up being deposited to the specified region on the wafer. The particle deposition efficiency as a function of radial distance is shown in Fig. 12. When the wafer-substrate plate is heated, there is no particle deposit onto the wafer for both 2.0 and 4.0 Torr pressures. However, when heating is not applied on the plate, particle deposition occurs. The deposition efficiency increases

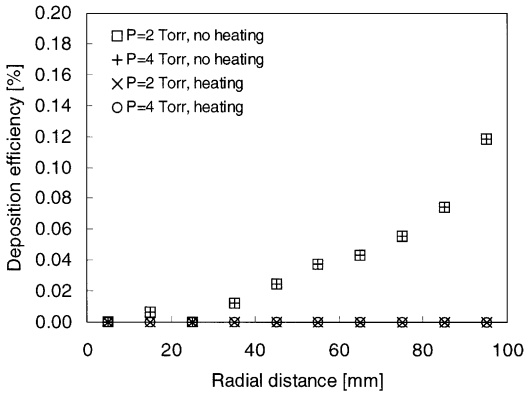

Fig. 12. Calculated deposition efficiency to the wafer-substrate plate as a function of radial distance for various conditions under study.

by increasing the radial distance. The trend is the same for pressures 2.0 and 4.0 Torr.

The effect of thermophoresis on particle trajectory in the space between the plates has been shown. As revealed by the simulation, by heating of the wafer-substrate plate, the flow patterns inside the entire reactor are quite different from those where no heating is applied except in the space between the plates, where a significant difference cannot be observed. This suggests that the change in particle trajectory in the space between the plates by heating of the wafer-substrate plate is primarily caused by thermophoresis. Both numerical and experimental results indicate that the thermophoretic force repels the particles from the wafer-substrate plate. However, it is not the wafer-substrate plate temperature that is important, but, rather, the temperature gradient between the wafer-substrate plate and the showerhead. Therefore, to minimize wafer contamination by minimizing particle deposition onto it the temperature gradient should be increased. Since, for a specific film deposition process, the temperature of the wafer is specific, raising the wafer temperature is nearly impossible. Therefore, the temperature gradient should be increased by reducing the showerhead temperature.

5. Conclusions

It has been demonstrated that the developed system of particle delivery from high pressure environment to low pressure chamber and of particle visualization has been used successfully to investigate particle transport and behavior in a low-pressure parallel plate CVD reactor. The visualization images of particle trajectories in the space between the plates using an LLS technique can be reproduced satisfactorily by a three-dimensional simulation by taking into consideration configuration details of the reactor. As revealed by both experiment and simulation, particle transport in the reactor is not influenced by pressure when the wafer-substrate plate is not heated. This differs from situations where in the wafer-substrate plate is heated, in which case the particle trajectories are strongly influenced. Simulations reveal that the change of particle trajectories as a result of heating the wafer-substrate plate, is primarily caused by thermophoresis effects.

Notation

C_c	Cunningham correction factor, dimensionless
C_m, C_s, C_t	constants in Eq. (5), dimensionless
d_p	particle diameter, m
$\mathbf{F}_D$	drag force, N
$\mathbf{F}_g$	gravity force, N
$\mathbf{F}_T$	thermophoretic force, N
K	ratio of the gas and particle thermal conductivities, dimensionless
Kn	Knudsen number, dimensionless
m_p	particle mass, kg
t	time, s
T	temperature, K
$\mathbf{u}$	gas velocity, m/s
$\mathbf{u}_p$	particle velocity, m/s
$\mathbf{x}_p$	particle position, m

Greek letters

μ	gas viscosity, kg/m s
ρ	gas density, kg/m^3

Acknowledgements

Y. Fujishige was very helpful in the experimental work. Support from Semiconductor Technology Academic Research Center (STARC), Japan is gratefully acknowledged. The financial support provided by the QUE project of Department of Chemical Engineering of Sepuluh Nopember Institute of Technology (ITS), Indonesia for H. Setyawan is gratefully acknowledged.

References

Adachi, M., & Okuyama, K. (1998). Particle deposition in air. in: Hattori (ed.), *Ultraclean surface processing of silicon wafers: Secrets of VLSI manufacturing* (pp. 67–81). Berlin: Springer.

Choi, S. J., Rader, D. J., & Geller, A. S. (1996). Massively parallel simulations of Brownian dynamics particle transport in low pressure parallel-plate reactor. *Journal of Vacuum Science and Technology A*, *14*(2), 660–665.

Collins, S. M., Brown, D. A., O'Hanlon, J. F., & Charlie, R. N. (1995). Postplasma particle dynamics in a gaseous electronic conference RF reference cell. *Journal of Vacuum Science and Technology A*, *13*(6), 2950–2953.

Fujimoto, T., Okuyama, K., Shimada, M., Fujishige, Y., Adachi, M., & Matsui, I. (2000). Particle generation and thin film surface morphology in the tetraethylorthosilicate/oxygen plasma enhanced chemical vapor deposition process. *Journal of Applied Physics*, *88*(5), 3047–3052.

Garrity, M. P., Peterson, T. W., Garret, L. M., & O'Hanlon, J. F. (1995). Fluid simulations of particle contamination in postplasma processes. *Journal of Vacuum Science and Technology A*, *13*(6), 2939–2944.

MacGibbon, B. S., Busnaina, A. A., & Fardi, B. (1999). The effect of thermophoresis on particle deposition in a tungsten low pressure chemical vapor deposition reactor. *Journal of The Electrochemical Society*, *146*(8), 2901–2905.

Nijhawan, S., McMurry, P. H., & Campbell, S. A. (2000). Particle transport in a parallel-plate semiconductor reactor: Chamber modification and design criterion for enhanced process cleanliness. *Journal of Vacuum Science and Technology A*, *18*(5), 2198–2206.

Oh, M. D., Yoo, K. H., & Myong, H. K. (1996). Numerical analysis of particle deposition onto horizontal freestanding wafer surfaces heated or cooled. *Aerosol Science and Technology*, *25*, 141–156.

Okuyama, K., Huang, D. D., Seinfeld, J. H., Tani, N., & Kousaka, Y. (1991). Aerosol formation by rapid nucleation in the preparation of SiO_2 thin film from $SiCl_2$ and O_2 gases using CVD process. *Chemical Engineering Science*, *46*(7), 1545–1560.

Okuyama, K., Huang, D. D., Seinfeld, J. H., Tani, N., & Matsui, I. (1992). Gas-phase nucleation in GaAs thin film preparation by MOCVD. *Japanese Journal of Applied Physics*, *31*(1), 1–11.

Patankar, S. V. (1980). *Numerical heat transfer and fluid flow*. London: Taylor & Francis.

Rao, N. P., Wu, Z., Nijhawan, S., Ziemann, P., Campbell, S., Kittelson, D. B., & McMurry, P. (1998). Investigation of particle formation during the plasma enhanced chemical vapor deposition of amorphous silicon, oxide, and nitride films. *Journal of Vacuum Science and Technology B*, *16*(2), 483–489.

Schmidt, F., Fissan, H., & Schmidt, K. G. (1996). Transport of submicron particles from a leak to a perpendicular surface in a chamber at reduced pressure. *Journal of Aerosol Science*, *27*(5), 739–750.

Slater, S. A., & Young, J. B. (2001). The calculation of inertial particle transport in dilute gas–particle flows. *International Journal of Multiphase Flow*, *27*, 61–87.

Talbot, L., Cheng, R. K., Schefer, R. W., & Willis, D. R. (1980). Thermophoresis of particles in a heated boundary layer. *Journal of Fluid Mechanics*, *101*(4), 737–758.

Ye, Y., Pui, D. Y. H., Liu, B. Y. H., Opiolka, S., Blumhorst, S., & Fissan, H. (1991). Thermophoretic effect of particle deposition on a free standing semiconductor wafer in a clean room. *Journal of Aerosol Science*, *22*(1), 63–72.